Electronic Properties of DNA Base Molecules Adsorbed on a Metallic Surface

Svetlana Kilina,[†,‡] Sergei Tretiak,[*,†,‡] Dzmitry A. Yarotski,[‡] Jian-Xin Zhu,[†] Norman Modine,[§] Antoinette Taylor,[‡] and Alexander V. Balatsky[†,‡]

Theoretical Division and Center for Nonlinear Studies (CNLS), Los Alamos National Laboratory, Los Alamos, New Mexico 87545, Center for Integrated Nanotechnologies, Los Alamos National Laboratory, Los Alamos, New Mexico 87545, and Center for Integrated Nanotechnologies, Sandia National Laboratory, Albuquerque, New Mexico 87545

Received: January 30, 2007; In Final Form: July 3, 2007

The internal electronic structure of single deoxyribonucleic acid (DNA) base molecules (i.e., guanine, adenine, cytosine, and thymine) adsorbed on a metallic surface of Cu(111) is determined in detail using density functional theory (DFT) computations. In contrast to the intuitive beliefs that a molecule weakly interacts with a substrate and its electronic structure is only slightly perturbed, our simulations reveal strong hybridizations and interactions between molecular and metallic states. Stipulated by the symmetries of a base molecule and the Cu(111) surface, oxygen atoms of a base approach close to the substrate, breaking the parallel orientation of the π-system with respect to the surface. Such a behavior is the most pronounced for one oxygen containing bases, leading to the chemisorption of cytosine and guanine and to stronger hybridization of their electronic states with metallic ones. Oxygen free adenine, on the other hand, lies nearly flat on a Cu substrate and interacts weakly with the surface through physisorption. The calculated local electron density of states spectra demonstrate the absence of pure localized molecular states for all four DNA bases, yet they show the smallest delocalization for adenine and thymine and the largest for guanine and cytosine. The observed diversity of the geometrical and electronic structures of the nucleobases on the Cu substrate provides guidelines for interpreting DNA tunneling spectra in the scanning tunneling microscopy (STM) measurements. Our results open a new prospective for understanding biomolecule adsorbates and have an important implication for a possible differentiation of nucleotide sequences in DNA through STM.

1. Introduction

Recently, we witnessed significant progress in a variety of experimental techniques targeted at imaging and resolving the structure and sequence of DNA and other biological molecules in faster and more cost-effective ways.[1] Two approaches that are often discussed in this context fall in two classes: (i) optical techniques, based on dideoxy methods,[2,3] and (ii) electronic methods, such as nanopores[4,5] and scanning tunneling microscopy (STM).[6,7] Whereas optical techniques are fairly well developed, electronic methods are very new approaches. They use local electronic probes to achieve resolution of better than 1 nm, which is necessary to identify the single DNA bases: adenine (A), cytosine (C), guanine (G), and thymine (T). A fundamental element of such an approach is the unique conductance through each of the DNA bases. Because the electronic and chemical structures of the four bases are intrinsically different, the electronic transport through each base should also be distinguishable, and it can be used to sequence DNA. These techniques show significant promise, yet far more exploration and development are needed if these techniques are to be routinely used in laboratories.

Among the questions that need more investigations, the nature of the interface and interaction of organic molecules with a metallic substrate is the central one. Metallic leads or conducting surfaces are the main components of the electronic methods. In the presence of a metal, the electronic structure of a DNA molecule often differs from that observed in the isolated case. Thus, the role of the hybridization of molecular orbitals with metallic states needs to be well understood to properly interpret the experiments. The question of the interaction between a molecule and metallic leads is also important for the design of molecular electronic nanodevices.[8−10] Here again, an adequate description of molecular electronic structure in the presence of metal is crucial to optimize electronic transport through a molecule and, thus, to achieve a proper functionality of such devices. It was also shown that transport through a DNA molecule varies strongly with the electrode−molecule arrangement.[11] This means that different nucleotides are distinguished by their conductance, largely because of their difference in size and in their orientation relative to the metallic contacts. It is still unclear whether DNA bases chemically bond to transition metals or only weakly interact with metal atoms through physisorption. Thus, both properties, the electronic structure and the geometrical position of a DNA base relative to the metallic contacts, need to be known to correctly characterize the charge transport through DNA.

In this paper we focus on the specific case of single DNA bases absorbed on a (111) oriented surface of copper. This study has been motivated by recent STM experiments performed by the Kawai group.[6,12−15] Their STM images of DNA bases deposited onto a Cu surface demonstrate the planar orientation of A bases on the surface and their one-dimensional (1D)

* To whom correspondence should be addressed. E-mail: serg@lanl.gov.
† Theoretical Division and Center for Nonlinear Studies, Los Alamos National Laboratory.
‡ Center for Integrated Nanotechnologies, Los Alamos National Laboratory.
§ Sandia National Laboratory.

10.1021/jp070805u CCC: $37.00
Published on Web 09/08/2007

aggregation through intermolecular hydrogen bonding. However, other bases self-assemble into clusters that have a much more intricate form than the 1D chains of the adenine, which complicates the interpretation of the base geometries. In addition to probing the molecular structure of DNA, STM allows one to simultaneously study the electronic properties of DNA bases. Thus, STM offers an approach where, in principle, the complete molecular mapping of DNA can be achieved. It was found[6] that the substrate density of states can affect the tunneling spectra of the adsorbed DNA molecule. However, the extent of this effect is still unclear. Our purpose is to determine how each individual nucleo-base is oriented onto the clean Cu(111) surface and how its electronic properties are affected by this surface.

On the basis of density functional theory (DFT), our simulations reveal: (i) a substantial hybridization between molecular levels and Cu states. Consequently, the presence of a metallic surface cannot be treated as a small perturbation on the electronic states of molecules, as was assumed in previous theoretical considerations.[12,13,15] (ii) The geometry optimization of DNA bases demonstrates a significant difference between A and T versus G and C molecules absorbed onto the metallic substrate. Particularly, the first two bases, and especially A, lay nearly flat on the Cu surface, whereas the other two bases are significantly tilted. The oxygens of the G and C bases closely approach Cu atoms, orienting the molecules to be almost perpendicular to the surface and providing coordination O−Cu bonding. (iii) Such a difference in geometries between adsorbed DNA bases is reflected by the preferential chemisorption of G and C bases over the physisorption of A and T molecules. (iv) There is a qualitative difference in the local density of states (LDOS) for A and T versus G and C. We have found that the LDOS of G and C has a substantially smaller peak for the highest occupied molecular orbital (HOMO) as compared to the lowest unoccupied molecular orbital (LUMO). This is because of the stronger hybridization of G and C molecular levels with metallic states, which in turn, is a result of stronger G and C bonding with the surface atoms. Our observations are in a good agreement with experimental results,[12,15] giving a new understanding of biomolecule adsorbates and a proper interpretation of available STM images of DNA.

This article is organized as follows. Details of our computational approach are presented in Section 2. In Sections 3.1 and 3.2 we analyze electronic structure of isolated DNA bases and their properties in the limit of weak interaction with metal surface, respectively. In Sections 3.3 and 3.4 we investigate geometry and electronic properties of DNA bases adsorbed onto Cu(111) and simulate possible STM spectra. Finally, we discuss the trends that emerge and summarize our findings in Section 4.

2. Methods and Simulation Details

In this paper we focus on two main questions: (i) the geometrical and electronic structures of each single DNA base molecule adsorbed on the Cu(111) surface, and (ii) the extent of interaction between the base and the Cu substrate. To investigate these questions numerically, the DFT is employed as the first principles quantum mechanical method. It provides efficient and typically accurate estimates of the energies of molecule−crystal binding, molecular dissociation, surface atom rearrangements, and the overall electronic structure of a system.[16−18] To our knowledge, only semiempirical methods were previously used for studies of DNA base self-assembly on the Cu surface.[12−15] The advantage of DFT is its ability to accurately treat d-electrons, which are important in transition metals such as Cu.

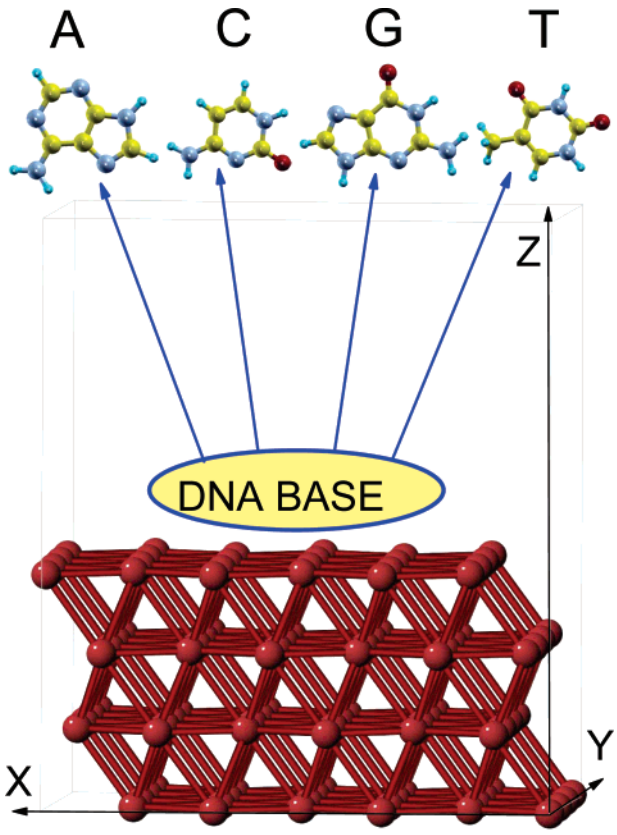

Figure 1. Schematic representation of the simulation cell used for the DFT calculations utilizing the plane-wave basis set and periodic boundary conditions. Red-brown color marks the copper atoms of the substrate (bottom of the scheme), Yellow, blue, red, and cyan colors represent carbon, nitrogen, oxygen, and hydrogen atoms in the various DNA bases, respectively (top of the scheme). Each simulation cell includes only one base molecule, initially laying flat with respect to the Cu(111) surface at the distance of around 3.5 Å from the substrate.

It is well-known that the DFT with a plane-wave basis set properly models electronic properties of bulk materials with Bloch-like wave functions spreading over the entire unit cell. However, finite size systems, such as organic molecules, are more efficiently described by the DFT with localized basis sets implemented, for example, by Gaussian functions. Yet, the system under consideration consists of both types of materials. Taking into account the dominant contribution of atoms from the metallic substrate, the plane-wave DFT within periodic boundary conditions has been chosen to investigate the interaction between the base molecules and the Cu surface as well as to model electronic properties of DNA bases in the presence of a substrate.

Plane-wave DFT simulations were performed with the VASP[19−21] code, which is particularly efficient for periodic metallic systems.[22−25] The core electrons were simulated using the Vanderbilt pseudopotentials,[26] and all valence electrons were treated explicitly. The generalized gradient functional of Perdew and Wang (PW91)[27] was used to account for the electron exchange and correlation effects. To describe the metallic nature of the sample, a grid of k-vectors was set up in the calculations. The grid included six *k*-points for each of the two directions along the surface and a single *k*-point in the direction perpendicular to the surface. The simulations were performed using plane-wave basis sets with over 10^6 plane-waves, corresponding to an energy cutoff of 396.0 eV (which is primarily required by highly electronegative species such as N and O).

The schema presented in Figure 1 illustrates the simulation

cell used for VASP calculations. The periodicity of the surface is essential to modeling the electronic structure of the metal. Therefore, the application of periodic boundary conditions along the *x*- and *y*-axes allows an accurate reproduction of the infinite close packed face-centered cubic (fcc) Cu(111) surface. The spurious periodicity in the direction perpendicular to the surface is suppressed by a 10 Å vacuum layer between the periodic images of the systems in the *z*-direction. The size of the cell along the *x*- and *y*-axes is dictated by the requirement of isolating the base from its periodic replicas, providing at least 4 Å between the molecule atoms and the cell boundaries. Thus, the simulation cell contains 96 copper atoms, consisting of a four-layer 6 × 4 periodically repeated slab of the Cu(111) surface and one DNA base.

The efficiency of DFT calculations of the proper equilibrium geometries strongly relies on a reasonable choice of the initial configuration of a system, which is used as the trial geometry for the geometry optimization procedure. For this purpose, the geometry of each DNA base/Cu composite was first fully optimized by classical molecular dynamics technique as implemented in the HyperChem software package.[28] The obtained geometries were further optimized using the VASP DFT package by minimizing the Hellmann−Feynman forces, using a conjugate gradient algorithm, until the total force on each ion converged to the 0.0005 eV tolerance limit. We allowed a full relaxation of the base molecule, as well as relaxation of the first layer of copper. This was essential for a proper account of the spatial anisotropy of the forces on the base molecule because of Cu atoms that contain d-electrons and form a continuous electronic band.

To check the validity of the chosen parameters, the VASP DFT geometry minimization procedure was first examined on a pure Cu(111) surface with the same simulation cell used for the combined molecule-metal system. The optimized Cu(111) system does not demonstrate any significant surface reconstructions when compared to the ideal bulk structure of the copper. That is in excellent agreement with experimental results[29] as well as with other numerical calculations of Cu(111).[30,31]

The next step was to check that the plane-wave DFT works as well for the finite system (the base molecules) as it does for the metallic surface. For this purpose, the DFT method implemented using the localized Gaussian basis set using the Gaussian 03 software package[32] was applied to each isolated DNA base molecule. The obtained results were compared to analogous calculations using the VASP DFT code. In these simulations, we focused on how well various models of density functionals reproduce the correct HOMO−LUMO gap for each nucleo-base. We employed the most commonly used functionals, specifically the gradient-corrected functional PW91 and three hybrid functionals: the Becke 3-parameter hybrid functional (B3LYP); the hybrid Perdew, Burke, and Ernzerhof functional (PBE1PBE); and the hybrid half-and-half functional (BHandH), which contain 20%, 25%, and 50% of the Hartree−Fock (HF) exchange, respectively. Calculations using the HF approach were conducted as well to explore the limiting case of 100% of the HF exchange. An extension of static DFT, time-dependent DFT (TD−DFT) coupled with the B3LYP functional, was also examined. TD−DFT is based on mapping of a TD interacting system to a non-interacting Kohn−Sham (KS) system with the same density, driven by an external perturbation.[33,34] It accounts for many-body effects in the TD exchange-correlation potential and allows inclusion of the Coulomb interactions and the correlation effects between excited electrons and holes, which is important for optical excitations of organic molecules.[35,36] A 6-31G basis set was used for all Gaussian calculations.

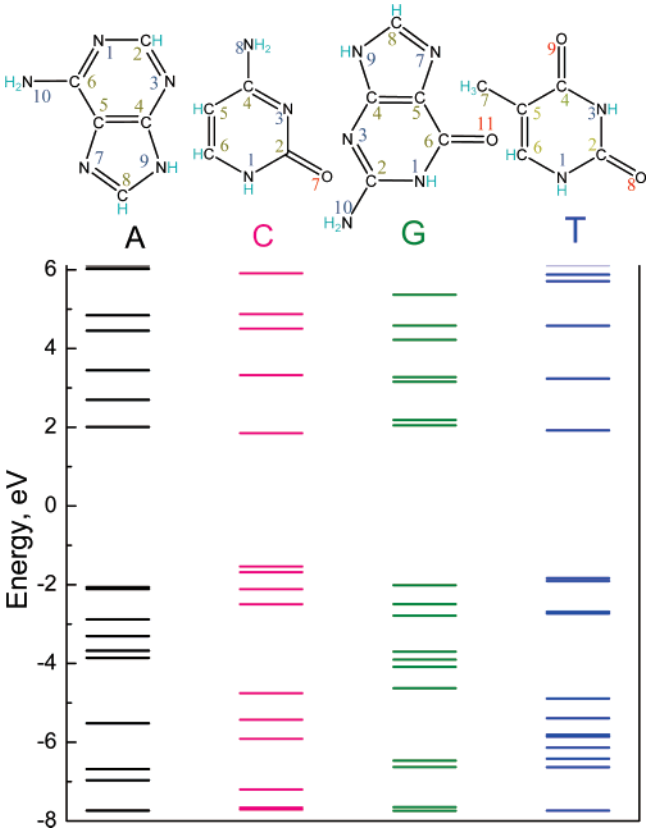

Figure 2. Schematic geometry (top panel) and electronic structure (bottom panel), calculated by PW91 functional using Gaussian software, is displayed for isolated bases: (A) adenine, (C) cytosine, (G) guanine, and (T) thymine. Shown numbering of base atoms stays unchanged for all other calculations. The energy of the guanine HOMO is noticeably shifted away from its valence band, which is a distinct feature compared to other DNA bases.

3. Results and Discussion

3.1. Electronic Structure of Isolated DNA Base Molecules. The optimized geometries and electronic structures calculated using the B3LYP functional are compared for all four isolated base molecules in Figure 2. These results confirm that all nucleobases have a large gap ($E_g \approx 5$ eV) and pretty similar electronic structures in the energy range around their LUMO−HOMO gaps. Only G has slightly different positions of the HOMO and LUMO, which distinguishes it from the other bases. Specifically, the energy spacing between the two LUMOs of G is around 0.1 eV, which is much smaller than for other base molecules. In contrast, the HOMO of G is separated by 0.6 eV from other occupied levels, whereas the energy spacing between the HOMO and the HOMO-1 for the other bases is almost half as large. These distinct features of the G valence band might explain the presence of a peak in the d*I*/d*V* STM spectrum, which was experimentally observed for G but not for other bases.[37]

Table 1 summarizes the values of the HOMO−LUMO gaps, obtained by different DFT functionals for all four bases, and compares the calculated results with available experimental and numerical data. The pure DFT functional PW91, in combination with either the Gaussian basis set or the plane-wave basis, produces very similar results. HOMO−LUMO gaps calculated with Gaussian basis set are slightly blue-shifted as compared to valued obtained in the plain-wave framework because of the incomplete 6-31G basis. In the latter case, the calculations

TABLE 1: HOMO−LUMO Gaps of Nucleobases Calculated by Different DFT Methods and Experimental First Optical Transitions[a,b]

DFT functional	E_{gap}^{A}, eV	E_{gap}^{C}, eV	E_{gap}^{G}, eV	E_{gap}^{T}, eV
HF	11.65	11.89	11.75	12.09
BHandHLYP	7.64	7.66	7.73	7.85
BPE1BPE1	5.70	5.63	5.82	5.81
B3LYP	5.31	5.21	5.59	5.41
TD-B3LYP	4.86	4.48	5.03	4.45
PW91(GAUS)	4.01	3.70	4.06	3.84
PW91 (VASP/GAUS geom.)	3.71	3.56	3.90	3.64
PW91 (VASP optimized)	3.81	3.52	3.83	3.74
TD-B3LYP (6-311++G**)[41]	4.98	4.64	4.96	4.99
experiment[41]	4.47 ± 0.02	4.46 ± 0.02	4.31 ± 0.02	4.64 ± 0.02
experiment[38−40]	4.51 − 4.63	4.40 − 4.70	4.31 − 4.59	4.44 − 4.8

[a] References 41, 41, 59, and 60. [b] Unless specified otherwise, the 6-31G basis set was used for all Gaussian calculations.

underestimate the band gaps of bases by roughly 1.5 eV. This is the standard systematic error of exchange-correlation functionals based on the adiabatic local density approximation (LDA) and gradient corrected functionals (GGA), such as PW91. The source of this failure is well-known: it is attributed to the lack of a derivative discontinuity in the LDA and GGA, stemming ultimately from the incomplete elimination of self-interaction by these functionals. Long-range nonlocal and nonadiabatic density functional corrections (such as hybrids including a portion of the exact HF exchange) are routinely used to remedy the problem. As can be seen from the Table 1, hybrid functionals lead to a consistent blue-shift of the energy gap. Larger amounts of the HF exchange present in the functional correspond to larger blueshifts. Overall, B3LYP provides the gap values closest to the experimentally observed ones.

Note that all DFT methods give the one-particle electronic gap, whereas in experiments, the lowest excitonic transition energy is measured. To get the transition energy, TD−DFT, which takes into account the effective attractive Coulomb interaction between photoexcited electron−hole pairs,[35] is applied. Because of the incorporation of many-body effects, TD-B3LYP calculations slightly reduce the one-electron energy gap, thus bringing the results into good agreement with experimental data. It is also necessary to note that experimental values of the first optical transitions vary significantly depending on the surrounding environment of molecules. Specifically, the base gaps are typically higher in the gas phase and aqueous solutions,[38−40] as compared to films.[41] The incomplete 6-31G basis set used for our calculations gives better gaps than the extended basis 6-311++G** with polarization and the diffuse functions used in ref 41. This likely results from the cancellation of errors because of an incomplete basis set and an imperfect density functional. Moreover, our calculations do not incorporate solvent effects that also need to be accounted for when comparing to experimental data. However, even with the reduced basis set, TD−DFT is numerically expensive and cannot be used for calculation of the large combined molecule−metal system, presented in Figure 1, when periodic boundary conditions are imposed.

Independent of the specific DFT functional, all of our calculations reproduce the delocalized π- and π*-character of the HOMO and LUMO for each isolated base molecule, as shown in Figure 3. Interestingly, the distribution of the wavefunction on the carbon−nitrogen rings of adenine and guanine is very similar for the HOMO, but is different for the LUMO. Cytosine and thymine differ much more in their wavefunctions for both the HOMO and LUMO. The similar π-like shapes of the wavefunctions obtained from Gaussian PW91 and plane-wave PW91, as well as the agreement in their HOMO−LUMO gaps for all four base molecules, demonstrate

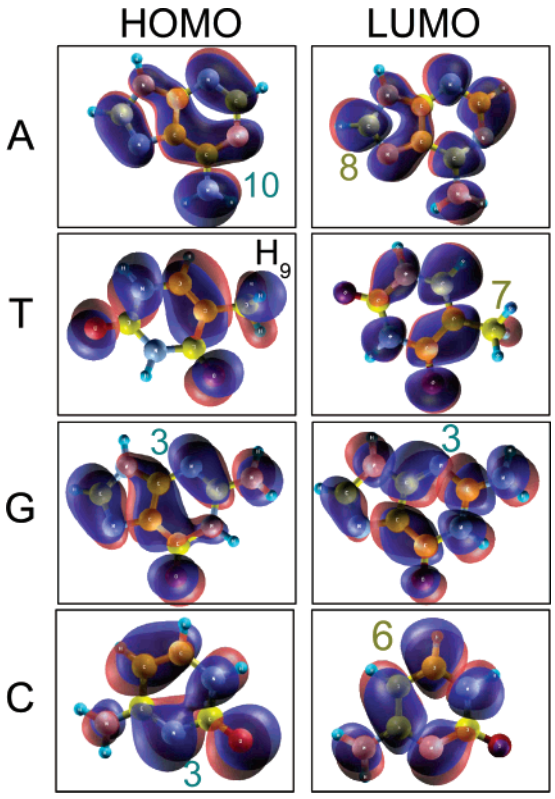

Figure 3. Highest occupied (HOMO, left panel) and lowest unoccupied (LUMO, right panel) molecular orbitals of A, T, G, and C calculated by B3LYP hybrid functional using Gaussian 03 software. Molecular orbitals are presented through surfaces of equal amplitudes of 0.02. The positive or the negative sign of the wave function is indicated by the red or blue color, respectively. We marked some atoms by numbered letters for an easier comparison of results from Table 3 and Figure 8

the validity of both localized and delocalized basis sets for modeling the electronic properties of finite organic systems. The underestimation of the gap by this functional can be later phenomenologically corrected by a "scissors" operator that shifts the unoccupied states to eliminate a systematic error.

On the other hand, proper representation of the base wavefunctions assures accurate geometry optimization, which is one of our main interests in the simulation of the base/Cu-substrate system. In general, both DFT methods, calculated using both plane-waves and Gaussian basis sets, provide a good agreement between optimized structures for isolated bases. For C, T, and G bases, PW91 DFT optimization gives slightly longer bond-lengths (ranging between 0.2% and 1.5%), as compared to VASP optimized ones. In the case of A, both methods result in nearly the same bond-lengths. The structure of G, optimized by VASP, demonstrates a strong pyramidalization[42] of the amino

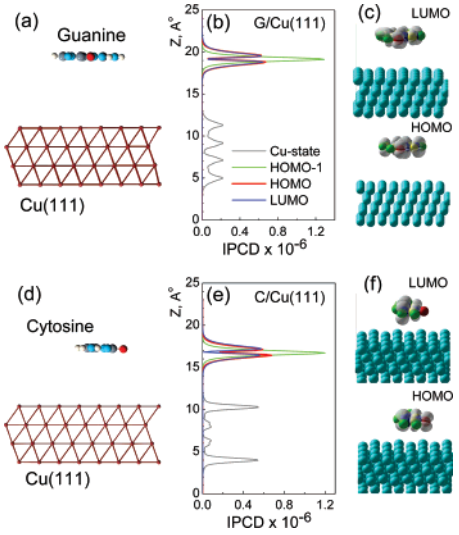

Figure 4. The structure of orbitals potentially contributing to the STM current. (a) Geometry of the G/Cu composite with the base placed far away from the metal surface; (b) relevant, integrated over *x*- and *y*-coordinates, partial charge density (IPCD) of G-specific HOMO-1, HOMO, and LUMO orbitals and metal-specific orbital energetically close to the G HOMO, as a function of the base−metal distance; (c) three-dimensional plots of the partial charge density of G-specific HOMO and LUMO. The same information is shown for the C base in plots d−f. Different electronic states of Cu were chosen for panels b and e to illustrate various features of metallic electron states. Thus, panel b corresponds to the pure bulk state, whereas panel e illustrates the electronic state of Cu mostly localized on the surface.

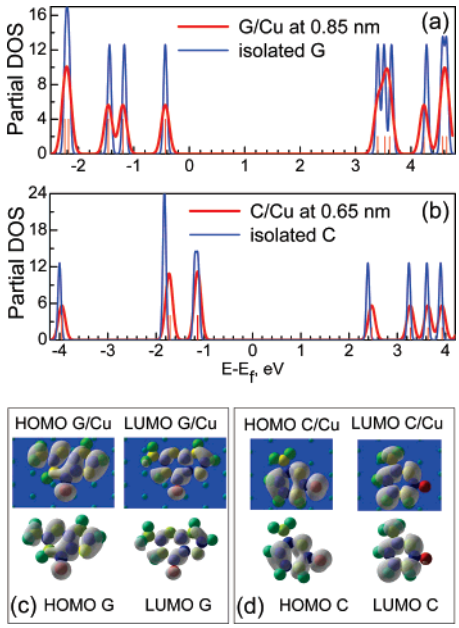

Figure 5. Partial density of states (DOS) of (a) G- and (b) C-specific molecular orbitals, compared to that of the G/Cu and C/Cu composites with the base placed very far from the metal surface. The red line corresponds to the base/Cu composite, and the blue line is attributed to the isolated G or C base. The molecular levels were separated from the continuum-states of the composite according to the localization of the partial charge density on a base-molecule. The relevant 3-D plots of the partial charge densities for HOMO and LUMO of the composites and isolated molecules are illustrated on panel c for G and panel d for C with isosurface values 0.01.

group, which originates from the balance between the sp^2-sp^3 hybridizations of the NH_2-group. The obtained angle between the plane made by the NH_2-group and the ring is 31.5°. It is in perfect agreement with previous calculations.[43,44] For other bases, both VASP and Gaussian calculations do not provide any noticeable pyramidalization. Although there is no clear direct experimental evidence about the nonplanarity of isolated bases, there is indirect evidence from vibrational transition moment measurements,[45] demonstrating a nonplanar A structure with the NH_2-group being tilted out of plane by ∼20°. However, it was reported that, in contrast to MP2 calculations,[46] a geometry optimization within B3LYP/6-311++G**[45] yields an essentially planar A structure. This issue challenges accuracy of modern DFT kernels and requires more detailed consideration in the future.

3.2. DNA Base Molecules Distant from the Cu(111) Surface. To investigate the influence of the Cu(111) surface on the electronic structure of DNA base molecules, we start from the case where a base is placed very far (7−9 Å) from the copper substrate. The positions of G and C molecules with respect to the surface are shown in Figure 4, panels a and d, respectively. At large distances, the interaction between the Cu surface and a nucleo-base should be negligible. Consequently, the electronic structure of a base stays the same as that of an isolated molecule. However, the combined base/Cu system is a metallic one, having a continuous electronic band. Some states from this continuum belong to a base molecule, others are metallic states. To identify the base molecular orbitals, partial charge densities $|\psi_n(r)|^2$ were calculated using the VASP software package. Here *n* corresponds to the index of the KS wavefunction ψ distributed over the electronic coordinater. Depending on whether the charge density of some specific state is localized either on the Cu substrate or on a base molecule (see Figure 4, panels c and f, respectively), this state is identified as either a metallic or a base state, respectively. For better illustration of these trends, Figure 4, panels b and e, presents the integrated partial charge density (IPCD) $\int dx \int dy|\psi_n(r)|^2$ and clearly distinguishes the metallic orbitals from the base orbitals. The complete localization of the charge density either on a base molecule or on Cu atoms indicates a negligible interaction between the metallic surface and the distant DNA base.

The absence of hybridization is also demonstrated by the coincident densities of states (DOS) of the base distant from the Cu surface and the isolated base, shown in Figure 5, panels a and b, respectively. In the case of C (Figure 5 b), the presence of the Cu surface disturbs the molecular levels more than for G (Figure 5 a). This is attributed to the smaller distance of 6.5 Å between C and Cu, as compared to 8.5 Å between G and the Cu surface. Less separation between the base and the surface leads to a slightly more pronounced effect of the Cu substrate on the electronic structure of C. For A and T bases placed at the distance of 8.5 Å from the surface (not shown), the DOS of the combined system does not demonstrate any significant deviations from the DOS of isolated bases. Overall, the very distant Cu substrate affects neither the electronic energies nor the wave functions of the base molecule (see Figure 5, panels c and d). On the other hand, when the base is adsorbed onto the surface, placing itself at a distance that minimizes the energy of the combined base/Cu system, the situation changes dramatically. Before discussing hybridization effects between the base and metallic states, the optimized geometry of the DNA base with respect to the surface has to be addressed.

3.3. Geometry of DNA Bases Adsorbed onto the Cu(111) Surface. The optimized structures of the four DNA bases on Cu(111) are presented in Figure 6, panels a, c, e, and g. This figure illustrates the side views of each system and indicates the proximity of a DNA base to the substrate, as well as its orientation with respect to the surface. Although we start with a similar parallel arrangement of each DNA base separated by

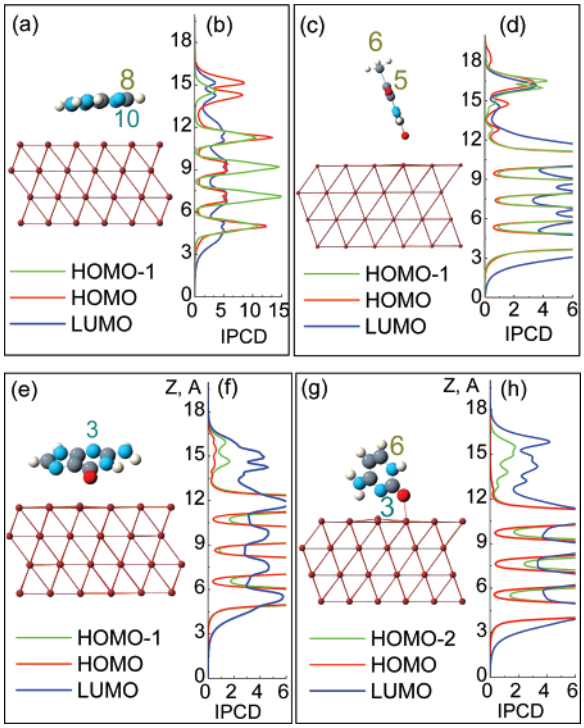

Figure 6. Optimized geometry and integrated partial charge densities (IPCD) of DNA bases adsorbed onto the Cu(111) surface: panels a and b, adenine; panels c and d, thymine; panels e and f, guanine; and panels g and h, cytosine. Here, gray, blue, red, and white colors indicate carbon, nitrogen, oxygen, and hydrogen atoms, respectively. The atoms, marked by numbered letters, correspond to the atoms from Table 3, which contribute the most to HOMO or LUMO LDOS peaks in Figure 8. Two major trends of the adsorbed bases are evident. Nitrogen-substituted aromatic rings tend to orient parallel to the surface, whereas oxygen atom (as shown in panels e and g) tend to approach the copper surface and form a coordination bond. The bonding is the most pronounced for G and C, leading to the strong hybridization of HOMO orbitals of these bases with metal ones.

3.5 Å from the surface (as classical molecular dynamics predicts), the final DFT optimized geometries are very different for the different DNA bases. Adenine, the only oxygen-free base, remains almost parallel to the Cu substrate at a distance of ∼3.2 Å. The nearly planar orientation of the A molecule provides the best overlap of the delocalized π-orbitals of its aromatic ring with the d-electrons of Cu. One of the important findings of our calculations is that the presence of the oxygen in the three other nucleobases results in significant deviations from a parallel orientation of these bases relative to the surface. This tilt allows oxygens to come closer to the copper atoms so that they can participate in the coordination bonding. Thus, in the cases of G, C, and T, there is an interplay between two competing processes. The π-structure of the base's aromatic rings favors a flat orientation of the base above the Cu substrate (to increase the overlap with Cu orbitals). On the other hand, oxygens try to approach Cu atoms as closely as possible to create coordination bonds. As a result, the molecular planes of these three bases exhibit a significant tilt angle relative to the substrate plane.

The nearly planar orientation of the A base on Cu(111) found in our simulations is confirmed by STM experiments.[12−15] STM images reveal that A on the Cu(111) surface self-assembles as a 1D chain structure with a topographic height of 0.2 nm.[14] Such a height is usually observed for π-systems lying flat on the Cu surface.[47] STM images of the other bases demonstrate more complicated self-assembled "islands", "squares", and "zigzags".[15] In particular, the diameter and height of bright spots that correspond to topographic images of T molecules appear to be completely random.[12] Thus, there is no clear STM evidence for pure 1- or 2-dimensional supramolecular structures of the C, G, and T bases. In other words, on the basis of our calculations, a parallel orientation of these bases on Cu(111) is not an adequate assumption. Results partially similar to our simulations were also observed for DNA bases adsorbed onto another surface (Si(111)) by means of spectroscopic ellipsometry and reflectance anisotropy spectroscopy.[41] Ellipsometry measurements show a mainly parallel orientation of A molecules with an average tilt angle of ∼10° with respect to the Si(111) surface, and G bases have larger tilt angles of ∼16°. The geometrically smaller T and C bases with only one aromatic ring demonstrate isotropic configurations on the Si surface, which does not allow them to specify their tilt angles.

To better understand individual features of the base adsorption onto Cu(111), we calculated the adsorption energy (or binding energy) E_{ads} for each base/Cu composite. Here we define E_{ads} as the difference between the total energy of the composite and the sum of the total energies of the free relaxed molecule and the surface: $E_{ads} = E_{base/Cu} - (E_{base} + E_{Cu})$. The respective adsorption energies, tilt angles, and maximum and minimum spacing between the molecule and metal atoms for each base/Cu system are summarized in Table 2. The observed negative values of E_{ads} for all four composites imply a stable adsorption of DNA bases onto the surface. This stability allows reproducible configurations of DNA molecules on the Cu(111) substrate that can be measured by STM.

We note that the T base, having two oxygens, demonstrates the lowest adsorption energy and the smallest tilt angle among the oxygen-containing bases. This is because the positions of the *O* atoms in T do not allow both oxygens to simultaneously approach the surface closely enough for chemical bonding with Cu atoms. The small tilt angle optimizes the mutual overlap of π-orbitals of the T aromatic ring and the wave functions of both oxygens with metallic orbitals. However, this configuration leads to such a weak interaction with the surface, that thymine physisorbs onto Cu(111) with the smallest binding energy, 0.2 eV. To check that the adsorbed T molecule was not trapped in a local minimum during geometry optimization, different ligations of the T to the surface have been also examined. As a starting configuration, T base was placed normally to the Cu surface with an O_8 atom located close to the surface at a distance of ∼2 Å, similar to the obtained O−Cu distances for adsorbed C and G bases. The final adsorbed configuration of the T base shows a significant tilted angle (∼60°) with respect to the surface and a slightly larger O−Cu distance of ∼2.4 Å (see Figure 6 c). However, the binding energy of this configuration increased only slightly (0.32 eV) as compared to the more planar configuration of T/Cu. The much smaller binding energies of both adsorbed configurations of the T molecule, as compared to adsorbed C and G bases, indicate a weak interaction of the T base with Cu atoms and its physisorption onto a metal substrate, independent of its parallel or normal orientation with respect to the surface.

Adenine also physisorbs onto the Cu substrate with a binding energy similar to the one of the normal configuration of the T/Cu composite. The obtained binding energy of A to the Cu(111) surface is in an excellent agreement with results calculated for A on a Cu(110) substrate,[48] where a weak interaction between A and the surface is also observed, despite the much closer location of a molecule with respect to the Cu atoms

TABLE 2: Geometry Parameters and Adsorption Energy of DNA Bases Adsorbed onto Cu(111)

	base atom	A/Cu	T/Cu (parallel)	T/Cu (normal)	G/Gu	C/Cu
maximum	C	3.62	3.98	7.43	3.78	5.07
distance	N	3.50	3.57	4.10	4.12	4.14
from the	H	3.69	4.81	8.04	4.33	6.05
surface, Å	O		3.46	6.44	2.16	2.08
minimum	C	3.21	3.66	3.37	2.78	2.83
distance	N	3.27	3.40	3.96	2.86	2.45
from the	H	3.10	3.10	3.47	2.90	2.07
surface, Å	O		3.13	2.24	2.16	2.08
angle, °		4	9	61	28	70
E_{ads}, eV		−0.34	−0.19	−0.32	−0.58	−1.34

(∼2.3Å) than in our case. Physisorption of A and T bases causes weak interaction between the molecule and the substrate, which in turn results in some flexibility of the molecule configuration on the surface. In the case of physisorption, small changes in the base configuration should not significantly change the total energy and adsorption energy of the system. Particularly, a decrease of the tilt angle, contributing to a more planar orientation of the base relative to the surface, changes the adsorption energy only on the order of ∼0.1−0.2 eV for both A and T bases. In contrast, the difference of adsorption energies for the initial flat and the final tilted configurations of C and G bases is much larger (∼0.4 eV) than that of A and T. Such a significant change in adsorption energies, depending on the base orientation relative to the surface, indicate chemisorption of C and G bases onto Cu(111). The short distance of ∼2 Å between the O and Cu atoms and the large binding energies of G/Cu and C/Cu (∼0.6 and ∼1.3 eV, respectively) provide more evidence of the chemisorption of these bases onto Cu(111) that occurs through the creation of a O−Cu coordination bond.

Unfortunately, there are no experimental data presently available on the adsorption energies to compare with our results. Despite the fact that the DFT methods include electronic exchange-correlation effects to some degree, the dispersion energy is not taken into account. Particularly, it was shown that GGA-DFT fails to describe the dispersion attraction of noble gases.[49,50] However, it was demonstrated that on distances of ∼2−3 Å the long-range dispersion interaction correction becomes negligible.[51] For example, binding energies and orientation of CH_4 adsorbed onto Ir(111), having a C−Ir distance of ∼2.5 Å, are calculated with reasonable accuracy by GGA-DFT.[51] In our case, because the calculated distances between base atoms interacting with the Cu surface are not larger than 3.5 Å, we assume that error due to the failure of the DFT calculations to account for van der Waals interaction is not very significant for our results.

On the basis of the fact that parallel and normal orientations of T with respect to the Cu substrate do not significantly change the binding energy and the character of the interaction between the base and metal atoms, we did not try normal configurations of A to the surface, predicting that these configurations also provide the physorption of A. Such an assumption is supported by numerical simulations for benzotriazole (a molecule similar to A and G but having all carbons in the hexagonal aromatic ring and three nitrogens in the pentagonal ring), reported in ref 52. The adsorption of this molecule onto Cu(111) predicts the base−metal interaction through overlapping of Cu d-orbitals with nitrogen sp^2 lone pairs. This interaction has a stronger character when the molecule is vertically standing on the copper surface rather than oriented parallel to the substrate. However, even in case of normal orientation of the molecule, its interaction with the surface cannot be considered as a strong one. In fact, the binding energy for benzotriazole/Cu is 0.43 eV,[52] which is slightly higher than that in our case for A/Cu and T/Cu systems, but it is noticeably lower as compared to C/Cu and G/Cu binding energies.

Because oxygen is a more electronegative element than nitrogen, it dominates the bonding with Cu for oxygen-containing DNA bases. By the same argument, the O−Cu coordination bond provides higher adsorption energy for C/Cu and G/Cu, as compared to the benzotriazole/Cu composite. However, the possibility of N−Cu bonding can be noticed for DNA bases adsorbed onto the Cu substrate. Particularly, in the C/Cu composite, one of the Cu atoms is sticked out from the surface toward the nitrogen in the C aromatic ring (see Figure 6 g), which demonstrates the trend of N−Cu bonding. The slight tilting of the A base toward the Cu surface also might be explained by a small amount of bonding between the nitrogen and Cu atoms. Nonetheless, our simulations demonstrate that for the base/Cu composites, chemisorption through the nitrogen is much less favorable than through the oxygen atoms.

However, the above reasons do not explain why the T base, with two oxygens, demonstrates physisorption on the Cu(111) surface, whereas other oxygen-containing bases are chemisorbed. To explain the dramatic difference of A/Cu and T/Cu adsorption versus G/Cu and C/Cu adsorption, additional analyses of changes in molecule structures due to adsorption and calculations of dipole moments of molecules were performed. Figure 7 compares the distortion of the base geometries when bases are adsorbed onto the surface. The physisorbed A base does not demonstrate any significant changes in its bondlengths, as compared to the isolated base, because of the very weak interaction with the surface. For chemisorbed C and G bases, there are noticeable decreasing of the C−NH_2 bond and increasing of the C−O bond, leading to more "double-character" of the C−NH_2 bond and more "single-character" of the C−O bond in these compounds. In turn, it brings a reorganization of more positive charge on the NH_2 group and more negative charge on the O atom. Such a distortion leads to a few changes in other double and single bonds in the aromatic ring to compensate the total charge on a base, thus creating new resonance structures of these molecules, as illustrated by Figure 7.

Note, that for the C base, the location of the NH_2 group near N_3 leads to the stronger localization of charge density near the nitrogen, as well. Thus, not only oxygen but also its neighboring nitrogen have an opportunity to effectively interact with Cu orbitals. Consequently, C should experience the strongest interaction with the surface among all other bases. Therefore, its binding energy is high. In the case of the G base, its N_3 atom is across from the oxygen, so that both of these atoms cannot be simultaneously close to the surface and interact with it. Therefore, the localization of charge density near N_3 is not as significant as for the C base. Nonetheless, the O atom in both the G and the C molecules is in a highly resonant bonding

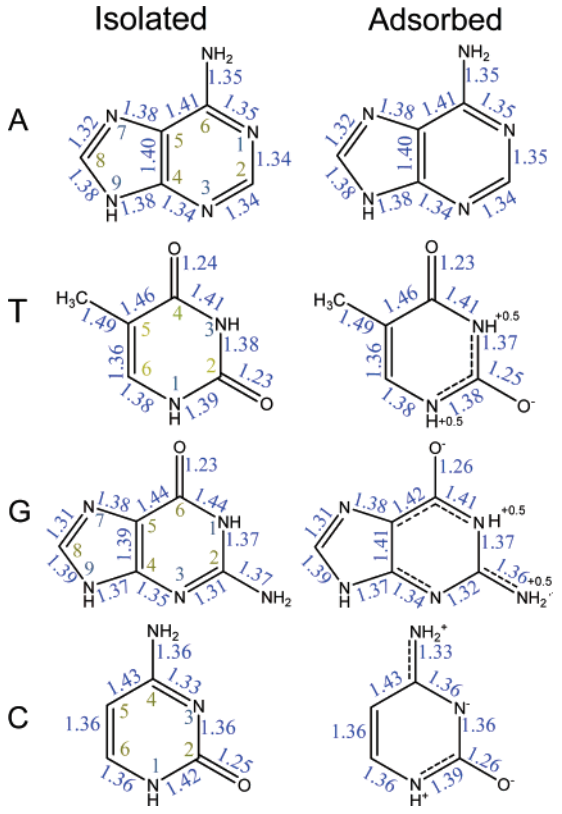

Figure 7. Schematic geometries and calculated bond length for isolated bases (left panel) and adsorbed bases on the surface (right panel). Only the normal orientation of adsorbed T base is displayed. For chemisorbed C and G bases, there are noticeable decreasing of the C−NH_2 bond and increasing of the C−O bond, assuming a reorganization of more positive charge on the NH_2 group and more negative charge on the O atom. Such a distortion leads to changes in other double and single bonds in the aromatic ring to compensate the total charge on a molecule, creating new resonance structures of these molecules. physisorbed A base does not demonstrate any significant changes in its bond length, as compared to the isolated base. For normally adsorbed T base, the overall change in bond length is much smaller than for C and G bases, demonstrating a weak interaction of this base with the surface.

configuration in which the bonds can rearrange to accommodate the formation of a new bond by O, which favors strong interaction of these bases with the Cu substrate.

In contrast, the T base does not have the amino group, which allows the rearrangement of the resonant bonds to terminate, as it occurs for C and G. Such a structural differences between T, on one hand, and C or G, on the other, explain the absence in our calculations of a chemisorbed T structure in which one of the O atoms in T forms a covalent bond to the Cu surface. In the T base, the O_8 atom has a non-resonant configuration, whereas the other O_7 atom has a weakly resonant configuration without the bond rearrangement terminating amino group. Furthermore, the weakly resonant O_7 atom in T has a bulky methyl group at a neighboring site, which may sterically hinder the formation of a bond between this O atom and the Cu surface. Therefore, for normally adsorbed T base and when O_8 is located very close to Cu atoms, the overall change in bond length is much smaller than for the C and G bases, demonstrating a weak interaction of this base with the surface.

In addition, the dipole moment of all four isolated bases were calculated. It is known that G and C bases are very polar molecules. For a C base, the calculated dipole moment is the largest one and is 7.04 D. The dipole moment of a G base is slightly smaller (6.98 D). The T base has an even smaller dipole moment (4.74 D), and the A base is the least polar base with dipole moment of 2.55 D. The experimental values of dipole moments of C and T are 6−6.5 D[53] and 4.14 D,[54] respectively. Depending on the basis set, the MP2 calculated[44] dipole moments of C, G, T, and A bases are 6.27−6.49, 6.45−6.65, 4.01−4.31, and 2.55−2.56 D, respectively. Our calculations are in perfect qualitative agreement with both experimental and theoretical data. The overestimation of the dipole moments, by ~0.5 D in the case of very polar bases, by our calculations probably originates from the ultra-soft potentials used in our DFT calculations. Polar molecules, such as the C and G bases, have a stronger tendency to interact with metal surfaces as compared to the less polar T and A bases. Therefore, C and G bases are chemisorbed, whereas A and T bases are physisorbed onto the Cu substrate. Consequently, the electronic structure of weakly interacting A and T bases should be only slightly disturbed by the presence of the substrate. In contrast, chemisorbed G and C bases strongly interact with the substrate, providing a strong hybridization between the base and metallic orbitals. Thus, their electronic structure should significantly deviate from that of the isolated G and C bases. We investigate this question in detail in the following section.

3.4. Electronic Properties of DNA Bases Adsorbed onto Cu(111). Prior to analyzing the influence of the copper surface on DNA bases, we identify which electronic levels of the composite system belong to the DNA molecule and which are associated with the metal. To single out the base molecular orbitals from the continuous electronic band of the base/Cu composite, the integrated partial charge density of each composite in its ground state was calculated in the same way described in Section 3.2. Unlike DNA bases placed far away from the surface, adsorbed bases do not have charge densities localized only on the molecule. Instead, there is some portion of the charge density on the base, as well as a significant portion distributed over the copper slab. Such a strong delocalization of molecular orbitals clearly indicates a strong hybridization between the base and metal states. Such base−copper hybridization makes the unique identification of molecular states impossible. In other words, after a DNA base is adsorbed onto the Cu(111) surface, there are no pure molecular states anymore but a quantum superposition of base and metal states, instead. Nonetheless, we identify the orbitals that can be approximately attributed to the base by finding a set of orbitals with the IPCD peaked on the base that also have energy spacings roughly coinciding with the spacings between the states of the isolated base.

Figure 6, panels b, d, f, and h, shows the distribution of IPCD over the *z*-coordinate for a few orbitals from the valence and conduction band edges that satisfy the above requirements. The IPCD of the bases' HOMOs demonstrates a qualitative difference between physisorbed and chemisorbed bases. Namely, the A and T bases physisorbed onto a copper surface have a pretty large portion of HOMO charge densities spread over the base. In contrast, the chemisorbed C and G bases display a dominant portion of the HOMO charge density concentrated on the copper slab and a relatively small part on the molecule. Such a distribution originates from the O−Cu bonding, which pulls the charge density toward the chemical bond, thereby bringing it closer to the surface. For C/Cu and G/Cu composites, molecular states lying below and above the HOMO have a much higher fraction of charge density concentrated on the molecule, as compared to the HOMO. This is because the HOMO electrons, rather than other molecular orbitals, are mostly responsible for chemical bonding. Also, the HOMOs of the isolated C and G bases (see Figure 3) demonstrate significant density localized

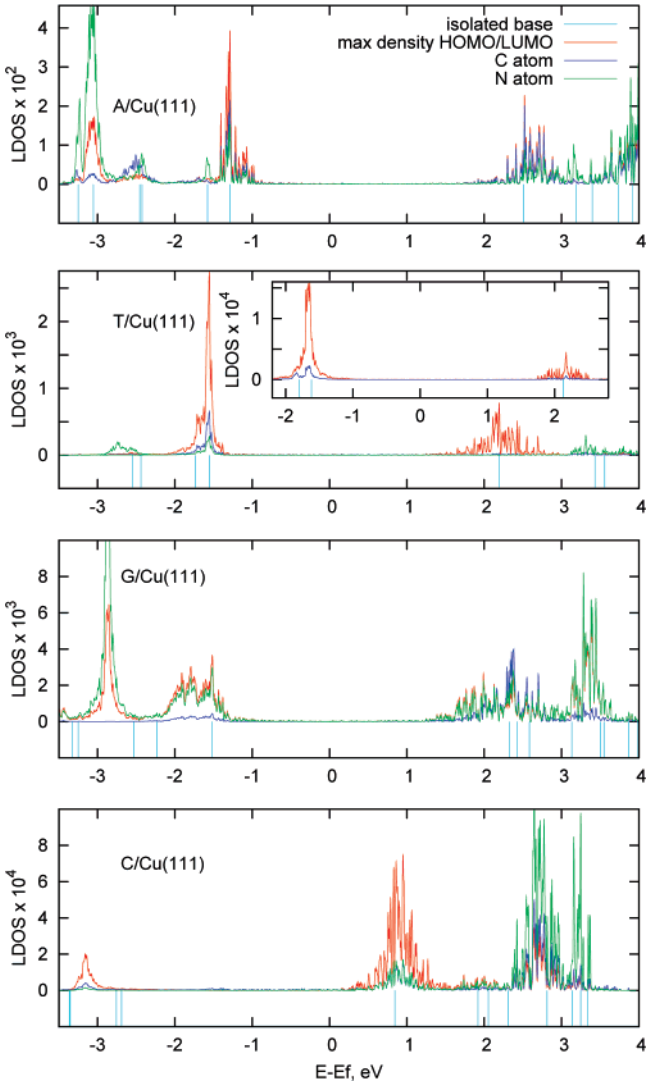

Figure 8. Local density of states (LDOS) of DNA base/Cu(111) composite calculated for the fixed Z-position (0.5 Å above the most distant base's atom from the surface) and varies *x*- and *y*-positions of the tip: above the highest C-atom (blue), above the highest N-atom (green), and the tip position providing the maximum LDOS (red). Note that the *x*−*y* tip position that optimizes the HOMO signal is used to obtain the red line for the filled state peaks, whereas the *x*−*y* position that optimizes the LUMO signal is used to obtain the red line for the empty state peaks. The energy levels calculated for simulation cells containing only isolated bases are presented by cyan vertical lines at the bottom of each panel and are for reference purposes. The four panels represent adsorbed A, T (parallel orientation), G, and C, respectively. The inset shows the LDOS for the normal orientation of T. For A and T composites, the LDOS peaks only slightly deviate from the electronic energies of the isolated bases, showing the small influence of the surface on the base electronic structure. For G and C composites, the deviation between their LDOS peaks and energies of free G and C bases is significant, pointing out the very strong interaction between those bases and the metal surface.

on oxygen atoms, which is necessary for bonding. Other molecular orbitals, for example, the LUMOs of both isolated C and G bases have a negligible amount of density on their oxygens. Therefore, the LUMOs (as well as the HOMO-1 and HOMO-2 states) of the C and G molecules are weakly involved in bonding and show much higher charge localization on the molecule as compared to the HOMO.

The major motivation for the present studies is the possibility of recognition of each individual base in DNA sequences by analyzing the related STM signals. A possible experimental procedure consists of two steps: First, a STM tip scans over the sample surface to find the positions that locally maximize the tunneling current at a fixed voltage. Second, the applied voltage sweeps through a range of values at the identified positions of the tip while the differential current is recorded. In this work, we numerically simulate the second stage: the voltage sweep revealing the details of the electronic structure of the sample. We calculated simulated STM images using the Tersoff−Hamann theory.[55,56] This theory is based on a *s*-wave approximation for the tip and a featureless tip density of states near the Fermi energy (ϵ_F). In this case (at zero temperature and tip−sample voltage bias V), the tunneling conductance dI/dV is assumed to be proportional to the LDOS $\rho(R_0, \epsilon_F + V)$ at the tip position R_0 and energy $\epsilon_F + V$. Thus, we simulate the STM spectra of DNA bases adsorbed onto Cu(111) by the LDOS calculated using KS wave functions and energies of the adsorbed systems (eq 1);

$$\frac{dI}{dV}(V) \sim \rho(R_0, \epsilon_F + V) = \sum_{i,k} |\psi_{ik}(R_0)|^2 \delta(\epsilon_F + V - \epsilon_{ik}) \quad (1)$$

where I is the current, and $|\psi_{ik}|^2$ and ϵ_{ik} are the VASP calculated wavefunction probabilities and the energies of the KS orbitals with state index i and wave vector k, respectively.

The calculated LDOS around ϵ_F, summed over all electron states in the energy window [−3.5;3.5] for each base/Cu composite, is presented in Figure 8. Because the spatial distribution of the wave function is different for different orbitals, the dominant contribution to the STM response might come from different base atoms for different composites. Taking this into account, for each base/Cu composite, we first fixed the *z*-coordinate of the tip position at 0.5 Å above the most distant atom from the surface. Next, at this fixed tip height, the tip position in the *xy*-plane that provides the maximum response (maximum LDOS) was found at voltages V corresponding to either the HOMO or the LUMO of a base adsorbed onto Cu(111). The LDOS values of both of the filled states, obtained at the *x*−*y* tip position that optimizes the HOMO signal, and of the empty states, calculated at *x*−*y* tip position optimal for LUMO signal, are shown by the red line in Figure 8. Positioning the tip at the same height, but above the nitrogen atom or carbon atom that is most distant from the surface (the green and blue lines in Figure 8, respectively), introduces new peaks in the STM spectrum, which correspond to other base levels. Thus, few different tip positions in the *xy*-plane at a fixed tip height allow computation of a more complete STM spectrum for each adsorbed DNA base.

We have also analyzed which base atom contributes to the HOMO and LUMO maxima in LDOS, and then we compared whether the HOMO and LUMO of a free base have a significant portion of their wave function concentrated on the same atom. Table 3 shows the results. Obviously, the main contribution to LDOS peaks should come from the atoms satisfying two conditions. First, a significant amount of wavefunction amplitude should be localized on the atom. Second, the atom is close to the tip; consequently, it is one of the more distant atoms from the surface. As can be seen from the table, the atoms that have a large concentration of the HOMO or LUMO wavefunctions in the free base (see Figure 3), contribute to the LDOS of the LUMO and HOMO of the composite when they are close enough to the tip. The exception is the C/Cu composite, which shows a HOMO contribution from N_3, which is close to the surface. This case can be explained by the shifting of charge density from the C molecule to the surface because of bond

TABLE 3: Atoms of DNA Bases Adsorbed onto Cu(111) That Give Maximum Contribution to LDOS Peaks Attributed to HOMO (LUMO) of Bases

		A/Cu	T/Cu (parallel)	T/Cu (normal)	G/Gu	C/Cu
HOMO	base atom	N_{10}	H_9	H_9	N_{13}	N_{11}
	tip distance, Å	0.63	0.41	0.48	0.64	4.02
LUMO	base atom	C_8	C_6	C_7	N_{13}	C_4
	tip distance, Å	0.51	0.91	1.05	0.64	1.40

formation with copper atoms. Because the N_3 atom of C/Cu is more distant from the tip as compared to the dominant atoms from other bases, the LDOS for its HOMO is much smaller in magnitude than for the other composites.

We note that all the STM-LDOS peaks have different intensities. Interestingly, the peaks for the physisorbed A and parallel T bases are higher (especially, in the case of A) than the peaks of the chemisorbed G and C bases, as well as physisorbed normal T. This can be explained by specifics of the orientation of each adsorbant molecule. A major contribution to the STM signal comes from the π-orbitals of the conjugated benzene-like rings, which extend into space far from the sample and toward the tip. For physisorbed bases, which are oriented mainly in a planar fashion, these π-orbitals are extended perpendicular to the copper surface, providing maximal contribution to the tunneling current. In the case of the chemisorbed bases, the π-orbitals are tilted with respect to the surface normal. Specifically, C is almost perpendicular to the copper substrate, so its π orbitals are almost parallel to the surface. Thus, a tilted orientation results in the charge density being localized closer to the surface and contributing less to the tunneling current. The same reasoning is true for decreased intensities of LDOS peaks for the normal orientation of the T base, as compared with the parallel T base. For instance, in the case of the normal T orientation (Figure 8, inset), the intensity of peaks is 10 times smaller than for the parallel orientation. Nonetheless, because of the weak interaction with the surface, the position of the HOMO and LUMO peaks for adsorbed T base pretty much coincide with the HOMO and LUMO energies of the isolated base, independent of the molecule orientation with respect to the surface. In contrast, LDOS peaks of adsorbed C deviate significantly from the energies of the isolated base. It originates from a strong interaction between C and the Cu surface.

Thus, from Figure 8, two major effects of the copper on the base electronic structure can be noticed. First, each orbital of a base is hybridized with many metallic orbitals. Because of such hybridization, the LDOS peaks related to specific base orbitals are significantly broadened. Second, not all LDOS peak centers coincide with the energy levels of the isolated bases. For the phyisorbed A and T bases (both parallel and normal orientations), most of the LDOS peaks appear near the energies of isolated base states. In contrast, for the chemisorbed C and G bases, the peak centers are noticeably shifted from the energies of the free C and G molecules. One of the reasons for such shifts in energy is a strong interaction of these bases with the surface, facilitated by the presence of O−Cu coordination bonds.

Also, our calculations demonstrate that the HOMO of A is noticeably shifted toward the Fermi energy of the composite. In STM conductance spectra, such a location of the HOMO corresponds to a peak at a smaller negative bias as compared to the positive bias for detecting the LUMO peak. The HOMOs of adsorbed T and G are also shifted toward the Fermi energy, but less strongly than that of A. In contrast, in C, the LUMO, but not the HOMO, is significantly shifted toward the Fermi energy. Thus, a smaller positive bias is needed to reach the LUMO peak as compared to the bias for HOMO observation. Such diversity in the electronic structure of DNA bases adsorbed on the Cu-substrate should be identifiable by STM measurements of the conductance spectra of DNA. This demonstrates the potential for differentiation of nucleotide sequences in DNA by STM.

4. Conclusions

In this paper, we have numerically addressed specifics of adsorption and STM spectra of each DNA base on the (111) copper surface. The calculations are based on DFT with the PW91 functional, a plane-waves basis set, and ultrasoft pseudopotentials. The STM spectra have been modeled using the Tersoff−Hamann approximation and the Kohn−Sham states of each base/Cu composite. To our knowledge, there have been no previous reports of DFT calculations of STM spectra for DNA bases on a metallic surface. We find that each base is adsorbed differently onto the substrate. In particular, A and T are adsorbed almost parallel to the Cu(111) surface with a tilt angle of less than 10°, if the starting structure was the parallel one.

Guanine and, especially, cytosine orient almost perpendicularly to the surface, having much larger tilt angles of ∼30° and ∼70°, respectively. The difference in the adsorption geometries leads to the weak physisorption of A and T (with adsorption energies of ∼0.3 and ∼0.2 eV, respectively) and to significantly stronger chemisorption of G and C onto Cu(111) through the formation of oxygen−copper coordination bonds (with adsorption energies of ∼0.6 and ∼1.3 eV, respectively).

Despite the qualitative difference in adsorption, the orbitals of all four bases are found to hybridize strongly with the orbitals of Cu atoms. This is seen from the substantial delocalization of the base partial charge density over the entire composite, instead of being localized only on a base. A significant broadening of peaks in the local density of states of the adsorbed DNA bases also indicates a strong base−metal hybridization. Consequently, our calculations demonstrate that the influence of the metallic surface on the electronic orbitals of DNA bases is strong.

This effect is even more pronounced in the case of chemisorbed G and C bases. The energy spacing between states of the isolated G and C bases deviates noticeably from the energy spacing between LDOS peaks attributed to the states of the adsorbed bases. Hence, for chemisorbed G and C bases, the interaction with the surface is very strong and cannot be treated as a small perturbation to either base orbitals or energies. In the case of physisorbed A and T bases, their STM peaks mainly coincide with the states of the isolated A and T bases. The energies of A and T molecules are only slightly perturbed by the presence of the copper surface, although base orbitals are strongly hybridized with copper orbitals.

Different equilibrium geometries of these molecules on the surface would lead to STM tunneling into different parts of the molecules. Because of the variety of base configurations with respect to the surface, as well as the diversity of base−surface interactions, variations in tunneling conductance through the individual DNA base should be observed. Thus, our results

confirms the potential for differentiation of nucleotide sequences in DNA through STM. A new understanding of bio-molecule adsorbates, the mechanism of DNA self-assembly on a metallic surface, and a proper interpretation of available STM images of DNA can be achieved using the theoretical approach developed here.

In addition to providing a theoretical foundation to the experimental STM observations on single nucleotides adsorbed onto a metal surface, our method demonstrates great promise in the areas ranging from DNA sequencing to molecular electronics. As mentioned before, transition of the DNA through a nanopore was proposed as one of the possible methods for nucleotide sequence determination.[5] In this method, the nanopore and a molecule in its center can be modeled by two tunneling junctions placed in series. Hence, our simulations may be applied directly to explain the dependence of the measured signal on the passing nucleotide, which will lead to an understanding of what voltage levels, nanopore geometry, and material to use to improve the speed and reliability of the method.

Uncovering the details of bond formation between nucleic-acids and metal electrodes may clarify the mystery of electrical conductivity of the DNA molecule, which is claimed to vary from that of an insulator and to being superconducting, depending on the way DNA is attached to the electrodes.[57] In-depth knowledge of metal-nucleotide interactions is of great interest for researchers working on development of the molecular electronic devices, since the exploitation of the DNA as a backbone for metal nanoparticle attachment holds a great promise for self-assembly of nanowires and single-electron transistors.[58]

Acknowledgment. The authors thank D. Cox, T. Kawai, N. Reich, H. Tanaka, A. Talin, and S. Trugman for valuable comments. S. K. thanks Oleg Prezhdo for fruitful discussions and the University of Washington Department of Chemistry for computer resources. The research was supported in part by the grants from DOE BES and LDRD. This work was performed in part at the US Department of Energy, Center for Integrated Nanotechnologies, at Los Alamos National Laboratory (Contract No. DE-AC52-06NA25396) and Sandia National Laboratories (Contract No. DE-AC04-94AL85000).

References and Notes

(1) Shendure, J.; Mitra, R.; Varma, C.; Church, G. *Nat. Rev. Genet.* **2004**, *5*, 335.

(2) Sanger, F.; Nicklen, S.; Coulson, A. R. *Proc. Natl. Acad. Sci. U.S.A.* **1977**, *74*, 5463.

(3) Hergenhahn, M.; Liu, Z. P. *Proc. Natl. Acad. Sci. U.S.A.* **2004**, *101*, 2963.

(4) Yan, H.; Xu, B. *Small* **2006**, *2*, 310.

(5) Fologea, D.; Gershow, M.; Ledden, B.; McNabb, D. S.; Golovchenko, J. A.; Li, J. L. *Nano Lett.* **2005**, *5*, 1905.

(6) Tanaka, H.; Kawai, T. *Appl. Surf. Sci.* **2006**, *252*, 5474.

(7) Tanaka, H.; Kawai, T. *Surf. Sci.* **2003**, *539*.

(8) Liu, F.; Wang, X. *Small* **2006**, *2*, 1356.

(9) Taniguchi, M.; Kawai, T. *Phys. E.* **2006**, *33*, 1.

(10) Ziemann, P.; Boyen, H. *Nat. Mat.* **2006**, *5*, 394.

(11) Zikic, R.; Krstic, P.; Zhang, X.; Fuentes-Cabrera, M.; Wells, J.; Zhao, X. *Phys. Rev. E.* **2006**, *74*, 011919.

(12) Furukawa, M.; Tanaka, H.; Kawai, T. *J. Chem. Phys.* **2001**, *115*, 3419.

(13) Furukawa, M.; Tanaka, H.; Kawai, T. *Surf. Sci.* **2000**, *445*, 1.

(14) Furukawa, M.; Tanaka, H.; Nakagawa, T.; Kawai, T. *Surf. Sci.* **1997**, *392*, 33.

(15) Tanaka, H.; Nakagawa, T.; Kawai, T. *Appl. Surf. Sci.* **1996**, *364*, 575.

(16) Puzdder, A.; Williamson, A. J.; Zaitseva, N.; Galli, G.; Manna, L.; Alivisatos, A. P. *Nano Lett.* **2004**, *4*, 2361.

(17) Barnard, A. S.; Curtiss, L. A. *Nano Lett.* **2005**, *5*, 1261.

(18) Chretien, S.; Gordon, M.; Metiu, H. *J. Chem. Phys.* **2004**, *121*, 9925.

(19) Kresse, G.; Furtmüller, J. *Phys. Rev. B.* **1996**, *54*, 11169.

(20) Kresse, G.; Hafner, J. *Phys. Rev. B.* **1996**, *49*, 14251.

(21) Kresse, G.; Furtmüller, J. *Comput. Mater. Sci.* **1996**, *6*, 16.

(22) Al-Lehyani, I.; Widom, M.; Wang, Y.; Moghadam, N.; Stocks, G. M.; Moriarty, J. A. *Phys. Rev. B.* **2001**, *64*, 075109.

(23) Speyer, G.; Akis, R.; Ferry, D. K. *J. Vac. Sci. Technol. B.* **2006**, *24*, 1987.

(24) Kilina, S. V.; Craig, C. F.; Kilin, D. S.; Prezhdo, O. V. *J. Phys. Chem. C.* **2007**, *111*, 4871.

(25) Cerny, M.; Boyer, R.; Sob, M.; Yip, S. *J. Comput.-Aided Mater. Des.* **2005**, *12*, 161.

(26) Vanderbilt, D. *Phys. Rev. B.* **1990**, *41*, 7892.

(27) Perdew, J. P. *Electronic Structure of Solids*; Akademie Verlag: Berlin, 1991.

(28) *HyperChem(TM) Lite v. 2.*; Hypercube, Inc.: 1115 NW 4th Street, Gainesville, Florida 32601, 1991.

(29) Kevan, S.; Gaylord, R. *Phys. Rev. B.* **1987**, *36*, 5809.

(30) Euceda, A.; Bylander, D.; Kleinman, L. *Phys. Rev. B.* **1982**, *28*, 528.

(31) Al-Rawi, A.; Kara, A.; Rahman, T. *Phys. Rev. B.* **2002**, *66*, 165439.

(32) Frisch, M. J.; Trucks, G. W.; Schlegel, H. B.; Scuseria, G. E.; Robb, M. A.; Cheeseman, J. R.; Montgomery, Jr., J. A.; Vreven, T.; Kudin, K. N.; Burant, J. C.; Millam, J. M.; Iyengar, S. S.; Tomasi, J.; Barone, V.; Mennucci, B.; Cossi, M.; Scalmani, G.; Rega, N.; Petersson, G. A.; Nakatsuji, H.; Hada, M.; Ehara, M.; Toyota, K.; Fukuda, R.; Hasegawa, J.; Ishida, M.; Nakajima, T.; Honda, Y.; Kitao, O.; Nakai, H.; Klene, M.; Li, X.; Knox, J. E.; Hratchian, H. P.; Cross, J. B.; Bakken, V.; Adamo, C.; Jaramillo, J.; Gomperts, R.; Stratmann, R. E.; Yazyev, O.; Austin, A. J.; Cammi, R.; Pomelli, C.; Ochterski, J. W.; Ayala, P. Y.; Morokuma, K.; Voth, G. A.; Salvador, P.; Dannenberg, J. J.; Zakrzewski, V. G.; Dapprich, S.; Daniels, A. D.; Strain, M. C.; Farkas, O.; Malick, D. K.; Rabuck, A. D.; Raghavachari, K.; Foresman, J. B.; Ortiz, J. V.; Cui, Q.; Baboul, A. G.; Clifford, S.; Cioslowski, J.; Stefanov, B. B.; Liu, G.; Liashenko, A.; Piskorz, P.; Komaromi, I.; Martin, R. L.; Fox, D. J.; T. K. *Gaussian 03, Rev. C.02*; Gaussian, Inc.: Wallingford, Connecticut, **2003**.

(33) Casida, M. E. *Recent Advantures in Density-Functional Methods Part I*; World Scientific: Singapore, 1995.

(34) Runge, E. Gross, E. K. U. *Phys. Rev. Lett.* **1984**, *52*, 997.

(35) Tretiak, S.; Igumenshchev, K.; Chernyak, V. *Phys. Rev. B.* **2005**, *71*, 33201.

(36) Tretiak, S. Mukamel, S. *Chem. Rev.* **2002**, *102*, 3171.

(37) Kawai, T. (unpublished).

(38) Voet, D.; Gratzer, W.; Cox, R.; Doty, P. *Biopolymers* **1963**, *1*, 193.

(39) Clark, L.; Tinoco, I. *J. Am. Chem. Soc.* **1965**, *87*, 11.

(40) Yamada, T.; Fukutome, H. *Biopolymers* **1968**, *6*, 43.

(41) Silaghi, S.; Friedrich, M.; Cobet, C.; Esser, N.; Braun, W.; Zahn, D. *Phys. Stat. Sol. (B.)* **2005**, *242*, 3047.

(42) Hobza, P.; Sponer, J. *Chem. Rev.* **1999**, *99*, 3247.

(43) Kydd, R.; Mills, I. *J. Mol. Spectrosc.* **1972**, *42*, 320.

(44) Roscioli, J.; Pratt, D. *Proc. Nat. Acad. Sci. U.S.A.* **2003**, *100*, 13752.

(45) Dong, F.; Miller, R. *Science* **2002**, *298*, 1227.

(46) Mishra, S.; Shukla, M.; Mishra, P. *Spectrochim. Acta A* **2000**, *56*, 1355.

(47) Stranick, S.; Kamna, M.; Weiss, P. *Science* **1994**, *266*, 99.

(48) Preuss, M.; Schmidt, W.; Bechstedt, F. *Phys. Rev. Lett.* **2005**, *94*, 236102.

(49) Wu, X.; Vargas, M.; Nayak, S.; Lotrich, V.; Scoles, G. *J. Phys. Chem* **2001**, *115*, 87484.

(50) von Lilienfeld, O.; Tavernelli, I.; Rothlisberger, U.; Sebastiani, D. *Phys. Rev. Lett.* **2004**, *93*, 153004.

(51) Henkelman, G.; Jonsson, H. *Phys. Rev. Lett.* **2001**, *86*, 664.

(52) Jiang, Y.; Adams, J. *Surf. Sci.* **2003**, *529*, 428.

(53) Bakalarski, G.; Grochowski, P.; Kwiatkowski, J.; Lesyng, B.; Leszczynski, J. *Chem. Phys.* **1996**, *204*, 301.

(54) Kulakowska, I.; Geller, M.; Lesyng, B.; Bolewska, K.; Wierzchowski, K. *Biochim. Biophys. Acta.* **1974**, *361*, 119.

(55) Tersoff, J.; Hamann, D. R. *Phys. Rev. Lett.* **1983**, *50*, 1998.

(56) Tersoff, J.; Hamann, D. R. *Phys. Rev. B.* **1985**, *31*, 805.

(57) Endres, R. G.; Cox, D. L.; Singh, R. R. P. *Rev. Mod. Phys.* **2004**, *76*, 195.

(58) Braun, G.; Inagaki, K.; Estabrook, R. A.; Wood, D. K.; Levy, E.; Cleland, A. N.; Strouse, G. F.; Reich, N. O. *Langmuir* **2005**, *21*, 10699.

(59) Matsuoka, Y.; Norden, B. *J. Phys. Chem.* **1982**, *86*, 1378.

(60) Novros, J.; Clark, L. *J. Phys. Chem.* **1986**, *90*, 5666.